Bistatic Integrated Sensing and Communication Scenarios with Transmitter and Receiver-Side Trade-Offs

Sebastian Fodor[♭], Gábor Fodor[⋆†], André L. F. de Almeida[◇], Miklós Telek[‡♯]
[♭]Stockholm University, Stockholm, Sweden. E-mail: sebbifodor@fastmail.com
[⋆]Ericsson Research, Stockholm, Sweden. E-mail: Gabor.Fodor@ericsson.com
[†]KTH Royal Institute of Technology, Stockholm, Sweden. E-mail: gaborf@kth.se
[◇] Federal University of Ceara, Brazil. E-mail: andre@gtel.ufc.br
[‡]Budapest University of Technology and Economics, Budapest, Hungary. E-mail: telek@hit.bme.hu
[♯]HUNREN-BME Information Systems Research Group, Budapest, Hungary. E-mail: telek@hit.bme.hu

***Abstract*—Previous works have investigated fundamental trade-offs in bistatic integrated sensing and communication (ISAC) systems, where the trade-offs are due to sharing the transmit resources between the sensing and communication signals. Interestingly, the ISAC trade-offs due to using an integrated multi-antenna receiver – where the communication and sensing signals cause interference to one another – are seldom studied. In this paper we study three bistatic ISAC structures, in which either the transmitter and/or the receiver serve as ISAC entities and study the transmit and receiver-side trade-offs and the achievable sensing and communication performance. In the fully integrated scenario, both the transmitters of the sensing and communication signals and the receiver of the two signals are integrated, which serves as a benchmark for the cases in which either the transmitters or the receivers of the sensing and communication signals are separated. Specifically, we derive the classical and the Bayesian Cramér-Rao bounds, which indicate that relaxing the transmitter and/or receiver-side trade-offs benefits both the sensing and communications performance at the expense of using more hardware, antenna, and transmit power resources. These analytical and numerical results can serve as a foundation for designing the architecture for bistatic ISAC networks. Based on these insights, we discuss some open questions that require further research.**

***Index terms*—** angle of arrival estimation, Cramér-Rao bound, integrated sensing and communication.

I. Introduction

Bistatic integrated sensing and communication (ISAC) has been proposed as the key enabler of perceptive cellular networks due to its ability to provide sensing services without full-duplex self-interference cancellation capabilities [1]–[5]. Specifically, the recent paper by Xiong et al. [3] considered the scenario in which the transmitting node (which is a multi-antenna base station (BS)) "splits" its transmit signal into communication and sensing signals (using a suitable multibeam or multilobe technique, see also [1], [4] and [6]), which are then processed by physically separate communication and sensing receiver nodes. In that model, consequently, the trade-off between communication and sensing is due to the limited power and antenna resources at the transmitter node. Note that in this scenario, there is no interference between the communication and sensing signals.

In contrast, in our previous paper [5], we investigated a bistatic ISAC system, in which both the transmitter node (a user equipment (UE) device) and the receiver (a multi-antenna BS) operate as a communication and sensing node. This arrangement is illustrated in Figure 1(a), which is characterized by a sum-power constraint at the UE and the communication and sensing signals causing interference to one another at the receiving BS. In that model, the ISAC trade-off is due to both the limited power resources at the transmitter and the limited antenna (spatial) resources at the receiver.

It is interesting to note that reference [3] assumes that the communication symbol is available at the sensing receiver, while the ISAC receiver studied in [5] estimates the communication symbol and the angle of arrival (AoA) from a passive object simultaneously. A variant of this scenario is when the transmitter node is a UE and the receiver nodes are BSs, as illustrated in Figure 1(b).

A third meaningful ISAC scenario is illustrated in Figure 1(c), in which the communication and sensing transmitter nodes are separated, but the receiving node (here, a multi-antenna BS) processes the received communication and sensing signals simultaneously. Note that in this case, the transmit-side power constraint can be relaxed since the two transmitters may set their respective power levels independently of each other. Here, an interesting case arises when the communication and sensing UE devices cooperate and do not necessarily transmit with full power in order to achieve some desired performance target at the ISAC BS.

Focusing on Scenario 2 (single ISAC transmitter), note that the paper [3] does not distinguish pilot and data signals for communications, whereas [5] explicitly distinguishes the pilot (channel state information at the receiver (CSIR) acquisition) and data transmission phases, where a sensing signal is transmitted in parallel with both the pilot and data

G. Fodor was supported by the 6G-MUSICAL EU Horizon 2023 project, Project ID: 101139176. M. Telek was supported by the OTKA K-138208 project of the Hungarian Scientific Research Fund. A. L. F. de Almeida acknowledges the National Council for Scientific and Technological Development (CNPq/Brazil) under grants 312491/2020-4 and 406517/2022-3.

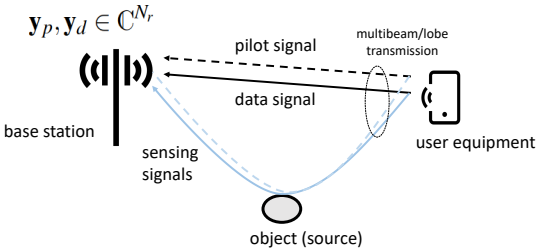

(a) Scenario 1

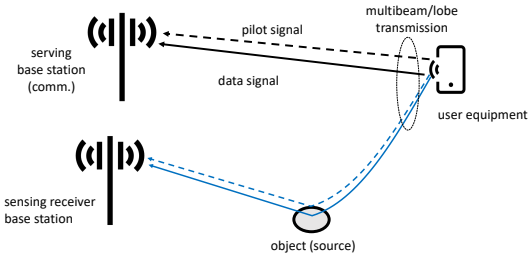

(b) Scenario 2

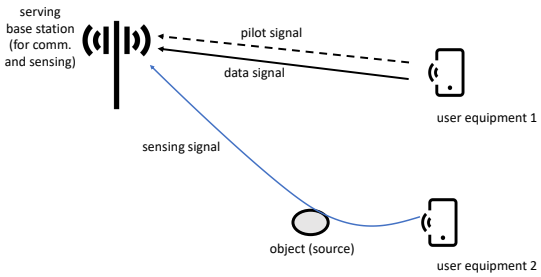

(c) Scenario 3

Figure 1: Integrated sensing and communication scenarios. The "fully integrated" scenario, in which both the transmitter and receiver nodes simultaneously transmit/receive communication and sensing signals, was investigated in our previous paper.

signals. In this paper, we study the three scenarios shown in Figure 1, and compare their performance in terms of the Cramér-Rao Bounds (CRBs) associated with AoA and symbol estimation, assuming unitary normalized constant envelope signaling. We ask the question whether separating the ISAC receiver or transmitter to two physical entities yields gains in terms of lower symbol estimation error at the communication receiver and improved AoA estimation at the sensing BS(s) compared with the performance of the fully integrated scenario 1(a) studied in [5], and what factors influence these performance gains. This question is motivated by the observation that separating the communication and sensing receivers requires more infrastructure resources, and it incurs some signaling and synchronization overhead to associate two BSs with the UE. On the other hand, it is intuitively clear that separating the receivers helps eliminate the interference between the communication and sensing signals, and we therefore study the beneficial effect in terms of lowering the CRBs.

Table I: System Parameters

Notation	Meaning
N_r	Number of receive antennas at the base station
$P_p,\ P_d,\ P_s$	Transmit power of pilot, data and sensing signals respectively
P	Number of objects (targets)
$\mathbf{p} \in \mathbb{C}^P$	Sensing signals from the P objects (referred to as sources in [7, Chapter 12])
θ_p	Angle of arrival of object p, $p = 1 \dots P$
$\mathbf{D} \in \mathbb{C}^{P \times P}$	Diagonal sensing matrix
$\mathbf{a}(\theta_p) \triangleq \left[\dots e^{\mathrm{i}\frac{2\pi}{\lambda} j\ell \sin(\theta_p)} \dots\right]^T \in \mathbb{C}^{N_r}$	Steering vector associated with θ_p, $j = 0 \dots N_r - 1$, where ℓ denotes the antenna spacing.
$\mathbf{A}(\boldsymbol{\theta}) \triangleq \left[\mathbf{a}(\theta_1) \dots \mathbf{a}(\theta_P)\right] \in \mathbb{C}^{N_r \times P}$	Steering matrix [7]
s	Transmitted uplink pilot symbol
x	Transmitted uplink data symbol
$\mathbf{h} \in \mathbb{C}^{N_r}$	Complex (effective) channel between UE-BS
$\alpha,\ \alpha_s$	Path loss between UE-BS and UE-object-BS (incl. radar cross-section of object)
$\mathbf{n}_p,\ \mathbf{n}_d \in \mathbb{C}^{N_r}$	Additive white Gaussian noise at the receiver (BS) when receiving the pilot and data signals
$\mathbf{C} \in \mathbb{C}^{N_r \times N_r}$	Stationary covariance matrix of the fast fading channel

II. System Model

A. Joint Receiver – Scenarios 1 and 3

The case when both the transmitter and receiver nodes are ISAC nodes – i.e., the transmitter can simultaneously transmit, while the receiver can simultaneously receive communication and sensing signals – was analyzed in our previous paper [5]. Specifically, we considered a single-user multiple input multiple output (SU-MIMO) bistatic ISAC system, in which the UE device transmits both sensing and communication (i.e., pilot or data) signals [1], [8], [9], see Figure 1(a). In general, there are P objects that reflect the sensing signals, which are collected by the P-dimensional $\mathbf{p}$ sensing vector. Following [7], we consider two models for the sensing vector. The deterministic model assumes that the source waveforms are non-random, while the stochastic model assumes that the waveforms are zero-mean Gaussian with covariance matrix $\boldsymbol{\Omega}$.

For the data transmission, we assume constant envelope unitary normalized signaling, that is x is uniformly distributed over the complex unit circle, $x = e^{\mathrm{i}\phi}$, where ϕ is a random variable with support $[-\pi, +\pi]$ [10], [11], [12].

The parameters characterizing this system are summarized in Table I. Under these assumptions, the received uplink spatially multiplexed sensing and communication signals are modeled as follows:

$$\begin{aligned} \mathbf{y}_p &= \mathbf{A}(\boldsymbol{\theta})\,\mathbf{D}\mathbf{p} + \alpha\sqrt{P_p}\mathbf{H}\mathbf{w}s^* + \mathbf{n}_p \ \in \mathbb{C}^{N_r}, \\ \mathbf{y}_d &= \mathbf{A}(\boldsymbol{\theta})\,\mathbf{D}\mathbf{p} + \alpha\sqrt{P_d}\mathbf{H}\mathbf{w}x + \mathbf{n}_d \ \in \mathbb{C}^{N_r}, \end{aligned} \tag{1}$$

where $\mathbf{p}$ contains the sensing signal; the communication is based on pilot signal s^* and data signal x; $\mathbf{H} \in \mathbb{C}^{N_r \times N_t}$ is the communication channel matrix between the UE device equipped with N_t transmit antennas and the serving BS equipped with N_r receive antennas; $\mathbf{w} \in \mathbb{C}^{N_t}$ is the transmit precoder at the UE; α denotes the path loss, and P_p and P_d denote the transmit power of the pilot and data signals respectively. In this paper, we assume that the UE operates single beamforming (see [10]) – in cellular systems also referred to as Rank-1 transmission [13], [14] – that is the UE transmits a single communication symbol x. While the multi-antenna UE transmits a single communication symbol x, it utilizes the multilobe technology to sweep a sensing sub-beam and illuminate targets of interest with controllable power, as proposed in, for example, [1], [15]. For ease of presentation, we will use $\mathbf{h} \triangleq \mathbf{H}\mathbf{w} \in \mathbb{C}^{N_r}$ to denote the uplink effective channel and re-write the received signal model as:

$$\begin{aligned} \mathbf{y}_p &= \mathbf{A}(\boldsymbol{\theta})\,\mathbf{D}\mathbf{p} + \alpha\sqrt{P_p}\mathbf{h}s^* + \mathbf{n}_p \ \in \mathbb{C}^{N_r}, \\ \mathbf{y}_d &= \mathbf{A}(\boldsymbol{\theta})\,\mathbf{D}\mathbf{p} + \alpha\sqrt{P_d}\mathbf{h}x + \mathbf{n}_d \ \in \mathbb{C}^{N_r}, \end{aligned} \tag{2}$$

where the diagonal sensing matrix, which collects the sensing path loss $\alpha_{s,i}$ and sensing power $P_{s,i}$ for each object, is defined as

$$\mathbf{D} \triangleq \begin{bmatrix} \alpha_{s,1}\sqrt{P_{s,1}} & \dots & 0 \\ \vdots & \ddots & \vdots \\ 0 & \dots & \alpha_{s,P}\sqrt{P_{s,P}} \end{bmatrix} \in \mathbb{R}^{P\times P}, \tag{3}$$

and $\mathbf{A}(\boldsymbol{\theta}) \in \mathbb{C}^{N_r \times P}$ is the steering matrix (see also Table I), and the effective communication channel follows the complex normal distribution $\mathbf{h} \sim \mathcal{CN}(\mathbf{0}, \mathbf{C})$.

Note that this signal model is an extension of the radar signal models used in [4], [7], [9], [16] by explicitly distinguishing the received pilot and data signals ($\mathbf{y}_p$ and $\mathbf{y}_d$). We will assume that the UE is equipped with multiple transmit antennas that enable it to divide its total transmit power between the communication (i.e., pilot and data) signals and the sensing signal, such that their sum $P_{\text{TOT}} \leq \max(P_p, P_d) + P_s$ remains under a power budget dictated by physical limitations and regulatory constraints [17].

B. Joint Transmitter with Separated Communication Receiver and Sensing Receiver – Scenario 2

In this scenario, the received signals at the communication and sensing BSs, respectively, can be written as:

$$\begin{aligned} \mathbf{y}_p &= \alpha\sqrt{P_p}\mathbf{H}\mathbf{w}s^* + \mathbf{n}_p \ \in \mathbb{C}^{N_r}, \\ \mathbf{y}_d &= \alpha\sqrt{P_d}\mathbf{H}\mathbf{w}x + \mathbf{n}_d \ \in \mathbb{C}^{N_r}, \end{aligned} \tag{4}$$

where $\mathbf{n}_p \sim \mathcal{CN}(\mathbf{0}, \sigma_p^2\mathbf{I}_{N_r})$ and $\mathbf{n}_d \sim \mathcal{CN}(\mathbf{0}, \sigma_d^2\mathbf{I}_{N_r})$, and

$$\begin{aligned} \mathbf{y}_{s_1} &= \mathbf{A}(\boldsymbol{\theta})\,\mathbf{D}\mathbf{p} + \mathbf{n}_{s_1} \ \in \mathbb{C}^{N_r}, \\ \mathbf{y}_{s_2} &= \mathbf{A}(\boldsymbol{\theta})\,\mathbf{D}\mathbf{p} + \mathbf{n}_{s_2} \ \in \mathbb{C}^{N_r}, \end{aligned} \tag{5}$$

where $\mathbf{n}_{s_1}, \mathbf{n}_{s_2} \sim \mathcal{CN}(\mathbf{0}, \sigma_s^2\mathbf{I}_{N_r})$. In this case, $\begin{pmatrix}\mathbf{y}_p \\ \mathbf{y}_d\end{pmatrix}$ is zero mean multivariate complex normal distributed with covariance matrix

$$\begin{aligned} \boldsymbol{\Psi}(\phi) &\triangleq \mathbb{E}\left[\begin{pmatrix}\mathbf{y}_p \\ \mathbf{y}_d\end{pmatrix}\begin{pmatrix}\mathbf{y}_p \\ \mathbf{y}_d\end{pmatrix}^H \middle| \phi\right] \\ &= \begin{pmatrix} \alpha^2 P_p\mathbf{C} + \sigma_p^2\mathbf{I}_{N_r} & \alpha^2\sqrt{P_pP_d}\mathbf{C}e^{-\mathrm{i}\phi} \\ \alpha^2\sqrt{P_pP_d}\mathbf{C}e^{\mathrm{i}\phi} & \alpha^2 P_d\mathbf{C} + \sigma_d^2\mathbf{I}_{N_r} \end{pmatrix}. \end{aligned} \tag{6}$$

Similarly, the vector of the received sensing signals is multivariate complex normally distributed with the following mean and variance. In the case of deterministic transmitted sensing signal, $\mathbf{p}$:

$$\boldsymbol{\mu}_d(\boldsymbol{\theta}) \triangleq \mathbb{E}\left[\begin{pmatrix}\mathbf{y}_{s_1} \\ \mathbf{y}_{s_2}\end{pmatrix}\middle|\boldsymbol{\theta}\right] = \begin{pmatrix}\mathbf{A}(\boldsymbol{\theta})\,\mathbf{D}\mathbf{p} \\ \mathbf{A}(\boldsymbol{\theta})\,\mathbf{D}\mathbf{p}\end{pmatrix}, \tag{7}$$

and

$$\boldsymbol{\Psi}_d(\boldsymbol{\theta}) \triangleq \mathbb{E}\left[\begin{pmatrix}\mathbf{y}_{s_1} \\ \mathbf{y}_{s_2}\end{pmatrix}\begin{pmatrix}\mathbf{y}_{s_1} \\ \mathbf{y}_{s_2}\end{pmatrix}^H \middle|\boldsymbol{\theta}\right] = \begin{pmatrix}\sigma_s^2\mathbf{I}_{N_r} & \mathbf{0} \\ \mathbf{0} & \sigma_s^2\mathbf{I}_{N_r}\end{pmatrix}, \tag{8}$$

where $\boldsymbol{\Psi}_d \triangleq \boldsymbol{\Psi}_d(\boldsymbol{\theta})$ is independent of $\boldsymbol{\theta}$. In the case of using a stochastic zero mean transmitted sensing signal, we have that $\boldsymbol{\mu}_s(\boldsymbol{\theta}) = \mathbf{0}$ and the covariance matrix is

$$\begin{aligned} \boldsymbol{\Psi}_s(\boldsymbol{\theta}) &\triangleq \begin{pmatrix}\mathbf{M}(\boldsymbol{\theta}) + \sigma_s^2\mathbf{I}_{N_r} & \mathbf{M}(\boldsymbol{\theta}) \\ \mathbf{M}(\boldsymbol{\theta}) & \mathbf{M}(\boldsymbol{\theta}) + \sigma_s^2\mathbf{I}_{N_r}\end{pmatrix} \\ &= \begin{pmatrix}\mathbf{A}(\boldsymbol{\theta})\,\mathbf{D} \\ \mathbf{A}(\boldsymbol{\theta})\,\mathbf{D}\end{pmatrix}\boldsymbol{\Omega}\begin{pmatrix}\mathbf{A}(\boldsymbol{\theta})\,\mathbf{D} \\ \mathbf{A}(\boldsymbol{\theta})\,\mathbf{D}\end{pmatrix}^H + \sigma_s^2\mathbf{I}_{2N_r}, \end{aligned} \tag{9}$$

where $\mathbf{M}(\boldsymbol{\theta}) = \mathbf{A}(\boldsymbol{\theta})\,\mathbf{D}\boldsymbol{\Omega}\mathbf{D}^H\mathbf{A}^H(\boldsymbol{\theta})$ and $\boldsymbol{\Omega} = \mathbb{E}[\mathbf{p}\mathbf{p}^H]$.

C. Fisher Matrix for Deterministic Sensing Signals

Recall that the CRB matrix is defined as the inverse of the Fisher information matrix (FIM) [18], and we therefore proceed with establishing the FIMs associated with ϕ and θ in the scenarios of interest. In the case of Scenario 1 and Scenario 3, the FIM is computed based on (2) and is provided in [5]. In this and the next subsection we focus on the separated receiver scenario (Scenario 2), which is characterized by (4) and (5) and to simplify the discussion we assume $P = 1$ target to sense and consequently, $\boldsymbol{\theta} = \theta_1$, $\mathbf{A}(\boldsymbol{\theta}) = \mathbf{a}(\theta_1)$. In Scenario 2 the FIM is defined as

$$\mathbf{I}(\phi) = -\mathbb{E}\frac{\partial^2}{\partial\phi^2}\log f_{\mathbf{y}_p,\mathbf{y}_d}(\mathbf{u},\mathbf{v}), \tag{10}$$

$$\mathbf{I}_d(\theta_1) = -\mathbb{E}\frac{\partial^2}{\partial\theta_1^2}\log f_{\mathbf{y}_{s_1},\mathbf{y}_{s_2}}(\mathbf{u},\mathbf{v}), \tag{11}$$

where $f_{\mathbf{y}_p,\mathbf{y}_d}(\mathbf{u},\mathbf{v})$ and $f_{\mathbf{y}_{s_1},\mathbf{y}_{s_2}}(\mathbf{u},\mathbf{v})$ stands for the density function of $\hat{\mathbf{y}}_c \triangleq \begin{pmatrix}\mathbf{y}_p \\ \mathbf{y}_d\end{pmatrix}$ and $\hat{\mathbf{y}}_s \triangleq \begin{pmatrix}\mathbf{y}_{s_1} \\ \mathbf{y}_{s_2}\end{pmatrix}$ with deterministic sensing signal. According to [5, eq. (13)] and [5, q. (15)]

$$\mathbf{I}(\phi) = \mathrm{tr}\left(\left(\frac{\partial^2}{\partial\phi^2}\boldsymbol{\Psi}^{-1}(\phi)\right)\boldsymbol{\Psi}(\phi)\right), \tag{12}$$

$$\mathbf{I}_d(\theta_1) = 2\left(\frac{\partial}{\partial\theta}\boldsymbol{\mu}_d(\theta_1)\right)^H\boldsymbol{\Psi}_d^{-1}\left(\frac{\partial}{\partial\theta}\boldsymbol{\mu}_d(\theta_1)\right). \tag{13}$$

since the $\mathbf{\Psi}(\phi)$ matrix in (6) is the same as in [5, eq. (7)]. Note that this implies that the Fisher information with respect to ϕ and θ_1 is equal in Scenario 1 and Scenario 2 (see also [5, eqs. (6), (13) and (15)]).

D. Fisher Matrix for Stochastic Sensing Signals

First, note that in the case of stochastic sensing signals, the Fisher information for ϕ, $\mathbf{I}(\phi)$, is the same as in the deterministic sensing signal case, since (4) does not depend on the sensing signal.

For $\mathbf{I}_s(\theta_1)$ (defined similar to $\mathbf{I}_d(\theta_1)$ but with stochastic sensing signal with $\boldsymbol{\mu}_s(\theta_1) = \mathbf{0}$ and $\mathbf{\Psi}_s(\theta_1)$), we need to determine the logarithm of the density function of $\hat{\mathbf{y}}_s$ with the stochastic sensing signal

$$\log f_{\mathbf{y}_{s_2},\mathbf{y}_{s_2}}(\mathbf{u},\mathbf{v}) = -\log \pi^{2N_r} \det \mathbf{\Psi}_s(\theta_1) - \left(\begin{pmatrix}\mathbf{u}\\ \mathbf{v}\end{pmatrix}^H \mathbf{\Psi}_s^{-1}(\theta_1) \begin{pmatrix}\mathbf{u}\\ \mathbf{v}\end{pmatrix}\right), \quad (14)$$

where

$$\begin{aligned}\det \mathbf{\Psi}_s(\theta_1) &= \det\left(\underbrace{\begin{pmatrix}\mathbf{a}(\theta_1)\,\mathbf{D}\\ \mathbf{a}(\theta_1)\,\mathbf{D}\end{pmatrix}}_{\mathbf{U}} \mathbf{\Omega} \underbrace{\begin{pmatrix}\mathbf{a}(\theta_1)\,\mathbf{D}\\ \mathbf{a}(\theta_1)\,\mathbf{D}\end{pmatrix}^H}_{\mathbf{V}^H} + \sigma_s^2 \mathbf{I}_{2N_r}\right)\\ &= \left(\sigma_s^2\right)^{2N_r} \det\left(\mathbf{I}_{2N_r} + \begin{pmatrix}\mathbf{a}(\theta_1)\,\mathbf{D}\\ \mathbf{a}(\theta_1)\,\mathbf{D}\end{pmatrix}^H \begin{pmatrix}\mathbf{a}(\theta_1)\,\mathbf{D}\\ \mathbf{a}(\theta_1)\,\mathbf{D}\end{pmatrix} \frac{1}{\sigma_s^2}\mathbf{\Omega}\right)\\ &= \left(\sigma_s^{4N_r}\right) \det\left(\mathbf{I}_P + \frac{1}{\sigma_s^2} \cdot\ 2 \cdot \mathbf{D}^H \mathbf{a}^H(\theta_1)\,\mathbf{a}(\theta_1)\,\mathbf{D}\mathbf{\Omega}\right),\end{aligned} \quad (15)$$

vanishes at the derivation according to θ_1, since $\mathbf{a}^H(\theta_1)\,\mathbf{a}(\theta_1) = N_r$. Furthermore:

$$\begin{aligned}\left(\mathbf{\Psi}_s(\theta_1)\right)^{-1} &= \left(\underbrace{\begin{pmatrix}\mathbf{a}(\theta_1)\,\mathbf{D}\\ \mathbf{a}(\theta_1)\,\mathbf{D}\end{pmatrix}}_{\mathbf{U}} \mathbf{\Omega} \underbrace{\begin{pmatrix}\mathbf{a}(\theta_1)\,\mathbf{D}\\ \mathbf{a}(\theta_1)\,\mathbf{D}\end{pmatrix}^H}_{\mathbf{V}} + \sigma_s^2 \mathbf{I}_{2N_r}\right)^{-1}\\ &\overset{(a)}{=} \frac{1}{\sigma_s^2}\left(\mathbf{I}_{2N_r} - \hat{\boldsymbol{\mu}}(\theta_1)\mathbf{B}^{-1}(\theta_1)\hat{\boldsymbol{\mu}}^H(\theta_1)\right),\end{aligned} \quad (16)$$

where $\mathbf{B}(\theta_1) \triangleq \left(\mathbf{\Omega}^{-1}\sigma_s^2 + 2\ \mathbf{D}^H \mathbf{a}^H(\theta_1)\,\mathbf{a}(\theta_1)\,\mathbf{D}\right)$ is not a function of θ_1 (since $\mathbf{a}^H(\theta_1)\,\mathbf{a}(\theta_1) = N_r$), $\hat{\boldsymbol{\mu}}(\theta_1) \triangleq \begin{pmatrix}\mathbf{a}(\theta_1)\,\mathbf{D}\\ \mathbf{a}(\theta_1)\,\mathbf{D}\end{pmatrix}$, and identity (a) is due to the Woodbury matrix identity. Using that $\mathbf{\Omega} = \Omega$, $\boldsymbol{\theta} = \theta_1$, $\mathbf{D} = D = \alpha_{s,1}\sqrt{P_{s,1}}$ are scalars, we get $\mathbf{B}(\theta_1) = B = \frac{\sigma_s^2}{\Omega} + 2N_r \cdot D^2$. Finally, utilizing

$$\mathbb{E}[\mathbf{z}^H\mathbf{A}\mathbf{z}] = \mathbb{E}\left[\mathrm{tr}(\mathbf{z}^H\mathbf{A}\mathbf{z})\right] = \mathbb{E}\left[\mathrm{tr}\left(\mathbf{A}\mathbf{z}\mathbf{z}^H\right)\right] = \mathrm{tr}\left(\mathbf{A}\mathrm{Cov}(\mathbf{z})\right),$$

with

$$\mathbf{z} = \begin{pmatrix}\mathbf{u}\\ \mathbf{v}\end{pmatrix} \text{ and } \mathbf{A} = \frac{\partial^2}{\partial\theta_1^2}\mathbf{\Psi}_s^{-1}(\theta_1), \quad (17)$$

we get

$$\mathbf{I}_s(\theta_1) = \mathrm{tr}\left(\left(\frac{\partial^2}{\partial\theta_1^2}\left(\mathbf{\Psi}_s(\theta_1)\right)^{-1}\right) \cdot \mathbf{\Psi}_s(\theta_1)\right), \quad (18)$$

Table II: Setting of the System Parameters

Parameter	Value
N_r	4
$\mathbf{C} = c\mathbf{I}_{N_r}$, with $c = 1$	Covariance matrix of the effective channel $\mathbf{h} = \mathbf{H}\mathbf{w}$.
$P_p,\ P_d,\ P_s$	Total power budget in Scenario 1 and 2: $P_p + P_s = 250$ mW; $P_d + P_s = 250$ mW.
P	1 (single object)
$\mathbf{p} \in \mathbb{C}^P$	$p = 1$ and $p \sim \mathcal{CN}(\mathbf{0}, \mathbf{\Omega})$, where $\mathbf{\Omega} = 1$ (scalar).
θ_p	Angle of arrival of object p, $p = 1 \ldots P$
s	$s = 1$
x	$x = e^{\mathrm{i}\phi}$, where $\phi \in [-\pi, \pi]$
$\alpha,\ \alpha_s$	60 dB ("low path loss, (PL)") or 80 dB ("high path loss, (PL)")

where the second derivative of $\left(\mathbf{\Psi}_s(\theta_1)\right)^{-1}$ can be computed from (16).

III. Numerical Results

In this section, we study the performance of the bistatic ISAC systems illustrated in Figure 1 in terms of the CRBs associated with the estimates of the symbol phase ϕ and AoA θ_1. We restrict our attention to the single object ($P = 1$) case and evaluate the performance assuming deterministic and stochastic sensing signals. The main system parameters are summarized in Table II. We note that the power budget constraint of scenario 1 and 2 is not applicable in scenario 3, which inhibits a fair comparison with scenario 1 and 2.

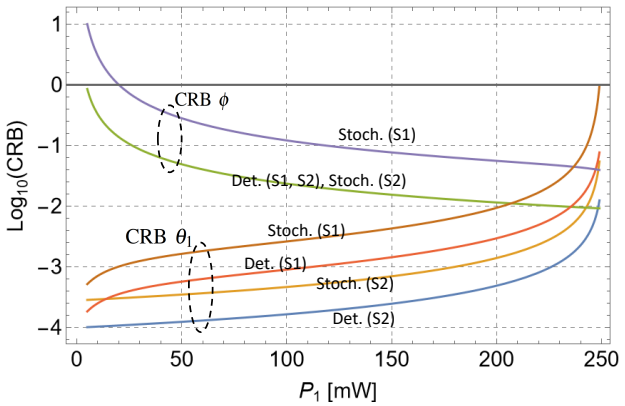

Figure 2: Comparing the achievable performance in Scenario 1 (S1) and Scenario 2 (S2) in terms of the CRBs for symbol ϕ and for AoA θ_1 in the deterministic and stochastic sensing waveform case with $P_1 \triangleq P_p = P_d$ and $P_s = 250\text{mW} - P_1$. As the communication power increases, the CRB for ϕ decreases, while the CRB for θ_1 increases due to the overall power budget in both scenarios.

Figure 2 compares the performance of Scenario 1 and Scenario 2. In both scenarios, the sum power budget during the pilot and data power slots must be maintained (see Table II). Therefore, the CRB associated with symbol estimation (ϕ) decreases as we increase $P_1 = P_p = P_d$, while the CRBs associated with AoA (θ_1) increase. Also, separating

the communication and sensing receivers in Scenario 2 helps to decrease the CRBs associated with θ_1. As it was noted at the end of Subsection II-C, and at the beginning of Subsection II-D, the CRBs associated with ϕ are the same in Scenarios 1 and 2 when using the deterministic sensing waveform and in Scenario 2 with the stochastic waveform.

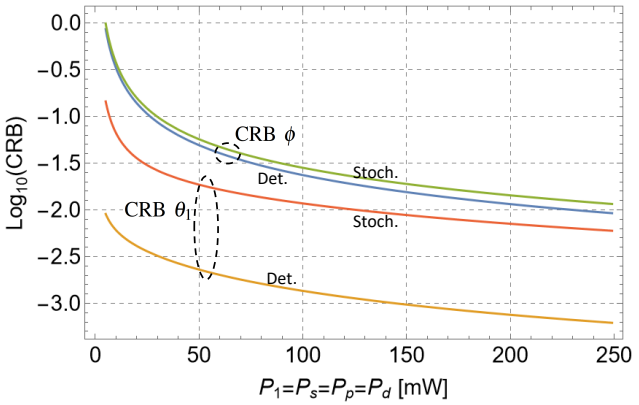

Figure 3: Achievable performance in Scenario 3 in terms of the CRBs for symbol ϕ and for AoA θ_1 in the deterministic and stochastic sensing waveform case with $P_1 \triangleq P_s = P_p = P_d$. That is, in this scenario, P_p, P_d, and P_s can be set independently from one another; here, we assume that they are set equally.

Figure 3 examines the performance in Scenario 3, in which the communication and sensing transmitters are separate UE devices. Therefore, in this scenario – unlike in Scenarios 1 and 2 – the communication (pilot and data) and sensing power levels can be set independently. In Figure 3, the communication and sensing power levels are set equally (indicated in the abscissa). Therefore, in this scenario, increasing $P_1 = P_s$ results in decreasing all CRBs. As expected, the CRB is lower when using the deterministic waveform than that associated with the random waveform.

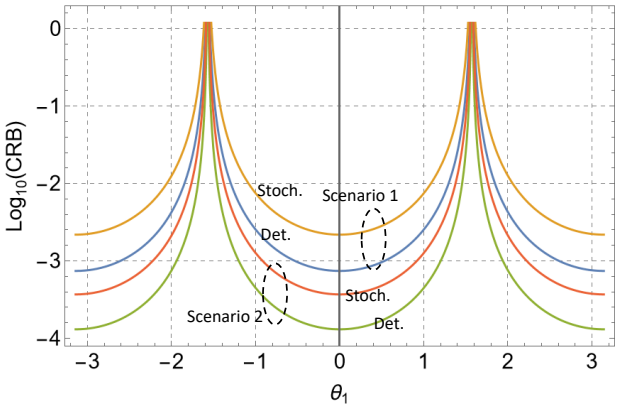

Figure 4: CRB for estimating θ_1 as a function of the true AoA (θ_1) in Scenario 1 and Scenario 2 using the deterministic and stochastic waveforms with $P_s = P_p = P_d = 125\,\text{mW}$. The AoA estimation error can be significantly lower in Scenario 2 than in Scenario 1 due to avoiding the interference between the sensing and communication signals.

Figure 4 shows the CRB for estimating θ_1 as a function of the true AoA in Scenarios 1 and 2. In both scenarios, the CRB gets low at $\theta_1 = 0$, which corresponds to the case when the impinging signal arrives from the boresight direction. In this case, the change in the phase difference at the antenna elements of the antenna array due to a small movement of the reflecting object is large – since the steering vector depends on the sine of θ_1 – leading to the lowest CRB.

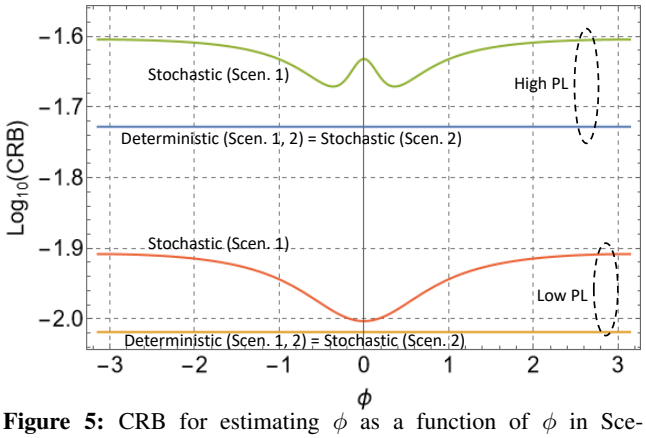

Figure 5: CRB for estimating ϕ as a function of ϕ in Scenario 1 and Scenario 2 using the deterministic and stochastic waveforms and assuming low or high path loss (PL) between the communication transmitter (UE) and the serving BS when $P_s = P_p = P_d = 125\,\text{mW}$. Note the CRB for ϕ is not a function of the true ϕ in Scenario 1 with deterministic waveform and in Scenario 2 with both the deterministic and stochastic waveforms.

Figure 5 shows the CRBs for estimating ϕ as a function of the true ϕ in Scenarios 1 and 2. The CRBs when using the deterministic waveform in both scenarios and when using the stochastic waveform in Scenario 2 are the same and independent of ϕ. On the other hand, the CRB depends on ϕ in Scenario 1 when using the stochastic sensing signal.

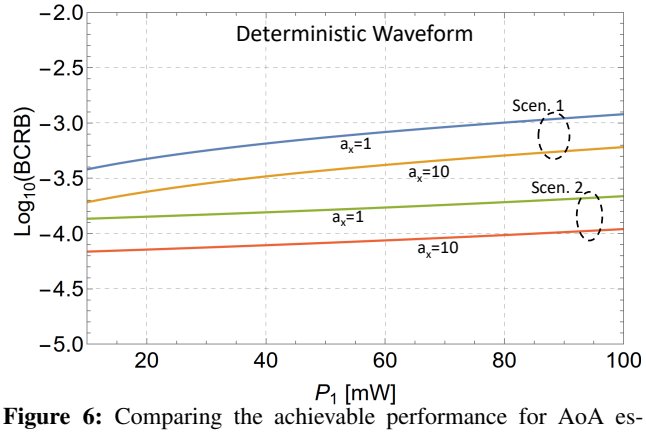

Figure 6: Comparing the achievable performance for AoA estimation in terms of the BCRB in Scenario 1 and Scenario 2 using the deterministic waveform with $P_1 \triangleq P_p = P_d$ and $P_s = 250\text{mW} - P_1$. Note that $a_x = 10$ corresponds to the case when more a priori information is available on the possible AoA than in the case of $a_x = 1$. As P_1 increases, the sensing power decreases in both Scenarios, which leads to increasing BCRB.

Figure 6 shows the Bayesian Cramér-Rao Bounds (BCRBs) as a function of P_1 in Scenarios 1-2 when using the deterministic sensing signal. The a priori information available about θ_1 is that θ_1 is uniformly distributed over $\left[0, \frac{\pi}{2a_x}\right]$ due to the geographic features of the environment,

where $a_x \geq 1$. Specifically, the BCRB plotted in this figure for Scenario 1 and 2 are defined as:

$$\tilde{\mathbf{I}}_{22}(a_x) \triangleq \frac{1}{2\pi} \cdot \frac{2a_x}{\pi} \int_{\phi=-\pi}^{\pi} \int_{\theta_1=0}^{\frac{\pi/2}{a_x}} \mathbf{I}_{22}(\phi, \theta_1)\ d\phi d\theta_1, \quad (19)$$

$$\tilde{\mathbf{I}}_{d}(a_x) \triangleq \frac{2a_x}{\pi} \int_{\theta_1=0}^{\frac{\pi/2}{a_x}} \mathbf{I}_{d}(\theta_1)\ d\theta_1. \quad (20)$$

As the figure shows, the BCRB decreases as the interval within which θ_1 lies decreases (as a_x increases from 1 to 10).

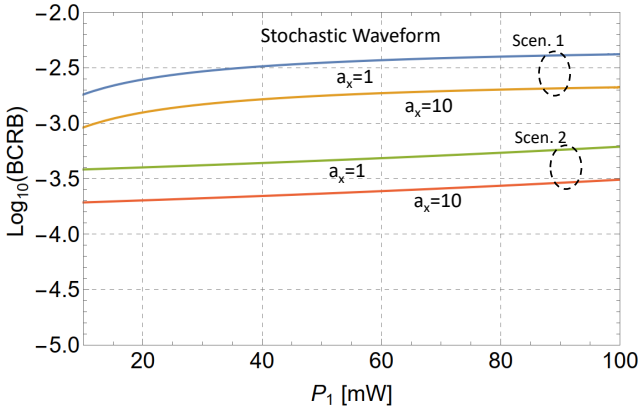

Figure 7: Comparing the achievable performance for AoA estimation in terms of the BCRB in Scenario 1 and Scenario 2 using the stochastic waveform with $P_1 \triangleq P_p = P_d$ and $P_s = 250\text{mW} - P_1$. Note that the BCRBs are somewhat higher than when using the deterministic waveform (see previous figure).

Finally, Figure 7 shows the BCRBs when using the stochastic waveform for sensing and using the same a priori information on θ_1 as in Figure 6. Notice that the BCRBs are similar to those in the deterministic waveform case, although they are somewhat higher in both scenarios. This is due to the fact that the CRBs are, in general, higher when using the stochastic sensing signal.

IV. Conclusions

In this paper, we studied the performance of bistatic ISAC systems, in which the integration of communication and sensing takes place either at the transmitter (Scenario 2) or at the receiver (Scenario 3) nodes, or at both of them (Scenario 1). When using the same receiver node as a communication and sensing receiver (Scenario 1 and Scenario 3), the sensing and communication signals cause interference with each other, which increases the CRBs for both sensing and communication. Scenario 2 benefits from separating the sensing and communication receivers at the expense of using additional hardware, which results in lower CRBs. The fully integrated scenario (Scenario 1) imposes constraints both at the transmitter (e.g., power budget) and at the receiver (due to reusing hardware and antenna) resources, which require the proper management of transmit resources and the design of multi-antenna ISAC receivers, which can deal with the interference caused by the sensing and communication signals to one another.

Our related future research plans include studying non-unitary signaling, multiple object sensing and precoding on the transmitter side.

References

[1] J. A. Zhang, X. Huang, Y. J. Guo, J. Yuan, and R. W. Heath, "Multi-beam for joint communication and radar sensing using steerable analog antenna arrays," *IEEE Transactions on Vehicular Technology*, vol. 68, no. 1, pp. 671–685, 2019.

[2] J. A. Zhang, M. L. Rahman, K. Wu, X. Huang, Y. J. Guo, S. Chen, and J. Yuan, "Enabling joint communication and radar sensing in mobile networks – A survey," *IEEE Communications Surveys and Tutorials*, vol. 24, no. 1, pp. 306–345, 2022.

[3] Y. Xiong, F. Liu, Y. Cui, W. Yuan, T. X. Han, and G. Caire, "On the fundamental tradeoff of integrated sensing and communications under Gaussian channels," *IEEE Transactions on Information Theory*, vol. 69, no. 9, pp. 5723–5751, 2023.

[4] M. U. Baig, J. Vinogradova, G. Fodor, and C. Mollén, "Joint communication and sensing beamforming for passive object localization," in *WSA and SCC 2023; 26th Int. ITG Workshop on Smart Antennas and 13th Conf. on Systems, Communications, and Coding*, 2023, pp. 1–6.

[5] S. Fodor, G. Fodor, and M. Telek, "On the trade-off between angle of arrival and symbol estimation in bistatic ISAC systems using Gaussian signaling," submitted for publication.

[6] C. B. Barneto, S. D. Liyanaarachchi, T. Riihonen, L. Anttila, and M. Valkama, "Multibeam design for joint communication and sensing in 5G new radio networks," in *ICC 2020 - 2020 IEEE International Conference on Communications (ICC)*, 2020, pp. 1–6.

[7] A. B. Gershman, *Array signal processing*. Cambridge University Press, 2006, pp. 241–260.

[8] F. Liu, C. Masouros, A. P. Petropulu, H. Griffiths, and L. Hanzo, "Joint radar and communication design: Applications, state-of-the-art, and the road ahead," *IEEE Transactions on Communications*, vol. 68, no. 6, pp. 3834–3862, 2020.

[9] G. Caire, C. R. C. M. da Silva, T. Gu, and W. Yuan, "Integrating sensing into communications in multi-functional networks," *IEEE Communications Magazine*, vol. 61, no. 5, pp. 24–25, 2023.

[10] J. Duplicy, J. Louveaux, and L. Vandendorpe, "Utility-based MIMO uplink beamforming," in *Fourth IEEE Workshop on Sensor Array and Multichannel Processing, 2006.*, 2006, pp. 254–257.

[11] L. C. Tran, A. Mertins, and T. A. Wysocki, "Unitary differential space-time-frequency codes for MB-OFDM UWB wireless communications," *IEEE Transactions on Wireless Communications*, vol. 12, no. 2, pp. 862–876, 2013.

[12] P. Singh, S. Srivastava, A. K. Jagannatham, and L. Hanzo, "Second-order statistics-based semi-blind techniques for channel estimation in millimeter-wave MIMO analog and hybrid beamforming," *IEEE Transactions on Communications*, vol. 68, no. 11, pp. 6886–6901, 2020.

[13] S. Yasukawa, T. Kawamura, Y. Kishiyama, H. Taoka, and T. Nakamura, "Experimental evaluation on SU-MIMO transmission with closed-loop precoding in LTE-Advanced uplink," in *2011 IEEE 73rd Vehicular Technology Conference (VTC Spring)*, 2011, pp. 1–5.

[14] S. Yasukawa, T. Kawamura, Y. Kishiyama, H. Taoka, and H. Andoh, "Influence of antenna configuration on achievable throughput in real indoor propagation environment for 2-by-2 single-user MIMO in LTE-advanced uplink," in *2012 International Symposium on Signals, Systems, and Electronics (ISSSE)*, 2012, pp. 1–6.

[15] K. Wu, J. A. Zhang, X. Huang, R. W. Heath, and Y. J. Guo, "Green joint communications and sensing employing analog multi-beam antenna arrays," *IEEE Comm. Mag.*, vol. 61, no. 7, pp. 172–178, 2023.

[16] C. Yuanhao, *Integrated Sensing and Communications*, F. Liu, C. Masouros, and Y. Eldar, Eds. Springer, 2023.

[17] 3GPP, "New Radio (NR): (UE) radio access capabilities," 3GPP, Technical Specification (TS) 38.306, 09 2023, version 17.6.0.

[18] S. M. Kay, *Fundamentals of Statistical Signal Processing, Vol. I: Estimation Theory*, ser. Prentice Hall Signal Processing. Prentice Hall, 1993, no. ISBN: 013-345711-7.